Appl Phys B (2010) 101: 623–629
DOI 10.1007/s00340-010-4247-8

Applied Physics B
Lasers and Optics

Enhancement of blue emission in β-$NaYbF_4$:Tm^{3+}/Nd^{3+} nanophosphors synthesized by nonclosed hydrothermal synthesis method

X.F. Wang · X.H. Yan · C.X. Kan · K.L. Ma · Y. Xiao · S.G. Xiao

Received: 3 December 2009 / Revised version: 30 July 2010 / Published online: 25 September 2010

Abstract An improved nonclosed hydrothermal synthetic processing is used to synthesize Tm^{3+} and Nd^{3+} doped β-$NaYbF_4$ nanophosphors at 85°C in the air without any high-temperature and high-pressure treatments as a final step. The particles have average crystallite size around 40 nm as obtained by TEM and calculation in terms of the XRD data. Intense 475 nm blue upconversion emission originated from the $^1G_4 \rightarrow {}^3H_6$ transition of Tm^{3+} is observed under 808 nm excitation, and its intensity can be enhanced onefold by introducing Nd^{3+} ion. The dominant populating mechanisms for the β-$NaYbF_4$:Tm^{3+} and β-$NaYbF_4$:Tm^{3+}/Nd^{3+} are thought as $Tm^{3+} \rightarrow Yb^{3+} \rightarrow Tm^{3+}$ and $Nd^{3+} \rightarrow Yb^{3+} \rightarrow Tm^{3+}$ energy transfer processes, respectively. The concentration quenching processes for blue and red emissions are discussed.

1 Introduction

With infrared solid-state lasers as a pumping source, a three-dimensional solid-state fluorescence display has been investigated extensively owing to its potentiality applications in television, computer aided design, air-traffic control, and medical imaging [1–6]. For applications, much attention has been dedicated to the exploration of strong and long lifetime blue, green, and red fluorescence emissions. The common method to produce intense blue emission is the $^1G_4 \rightarrow {}^3H_6$ transition of Tm^{3+} ion though an upconversion process. The compact, inexpensive, and power-rich near-infrared commercial diode lasers are employed as pumping resources to exploit blue emission of Tm^{3+}. The blue and red upconversion emissions of Tm^{3+} were obtained in Yb^{3+}–Tm^{3+} co-doped glass and powders under 980 nm excitation [7–11], Ta_2O_5 waveguides under 793 nm excitation [12], $LiNbO_3$ crystals under 795 nm excitation [13], tellurite-germanate glass under 798 nm excitation [14], and $PbGeO_3$–PbF_2–CdF_2 doped glass under 800 nm excitation [15], respectively. However, to our knowledge, it is rarely reported that strong blue monochromatic emission originated from Tm^{3+} in fluoride crystals excited by a power-rich 808 nm commercial diode laser.

The fluoride crystals with low phonon energy and high chemical stability are being adopted as the best upconversion candidate hosts for applications in solid-state lasers and biomedical images [16–25]. Especially, the hexagonal $NaYF_4$ doped with Yb^{3+}, Tm^{3+}, and Er^{3+} has been reported as the most efficient materials as biomedicine probes to realize red, green, and blue upconversion luminescence for detection of DNA and avidin [18, 19, 21–24]. Among the fluoride crystals, the β-$NaYbF_4$ crystals is unique, because it has similar crystal structure with hexagonal $NaYF_4$, and may offer sufficient Yb^{3+} with long excited level life as energy-transfer bridging ion between an energy donor ion R_1^{3+} ($R_1^{3+} = Tm^{3+}$ or Nd^{3+}) and acceptor ion R_2^{3+} ($R_2^{3+} = Tm^{3+}$, Er^{3+}, Ho^{3+}, or Tb^{3+}) to carry out energy transfers process $R_1^{3+} \rightarrow Yb^{3+} \rightarrow R_2^{3+}$ under 808 nm excitation. The reported methods used to synthesize β-$NaLnF_4$ (Ln = Y, Yb, Er, and Eu) crystals are high-temperature solid-state reaction, coprecipitation, and hydrothermal synthesis methods

X.F. Wang · X.H. Yan (✉) · C.X. Kan · K.L. Ma · Y. Xiao
College of Science, Nanjing University of Aeronautics and Astronautics, Nanjing 211106, People's Republic of China
e-mail: xhyan@nuaa.edu.cn

X.F. Wang
e-mail: wxf@nuaa.edu.cn

S.G. Xiao
Institute for Nanophysics and Rare-earth Luminescence, Xiangtan University, Xiangtan 411105, People's Republic of China

[21–27]. The above methods contain some limited experimental conditions as a final step, such as high-temperature process, high pressure, and HF atmosphere to avoid possible contamination from oxygen. Thus, it is necessary to exploit a soft chemistry route for preparing fluoride crystals without any high-temperature thermal treatment, high pressure, and HF atmosphere.

In Li's work [28], a novel nonclosed hydrothermal synthetic processing is reported to synthesize rare-earth doped α-$NaYF_4$ nanophosphors at 160°C for 2 hours. In this work, the nonclosed hydrothermal synthetic processing is improved to synthesize Nd^{3+}–Tm^{3+} codoped β-$NaYbF_4$ nanophosphors at 85°C in the air. The enhanced blue (475 nm) emission of Tm^{3+} is observed under 808 nm excitation, and possible mechanisms involved in the observation are discussed.

2 Experiment

All the chemical reagents were used without further purification. A typical procedure of the nonclosed hydrothermal synthetic method for preparing β-$NaYbF_4$:0.8%Tm, 0.2%Nd sample is as follows: in the first step, the Rare earth oxides Yb_2O_3 (99.99%), Nd_2O_3 (99.99%), and Tm_2O_3 (99.99%) were dissolved in adequate hydrochloric acid. The mixed aqueous solution containing $YbCl_3$, $NdCl_3$, and $TmCl_3$ was added into a beaker according to the molar composition of $NaYb_{1-0.008-x}Tm_{0.008}Nd_xF_4$ ($x = 0.2\%$). An adequate amount of NH_4HF_2 aqueous solution was added slowly into the solution as precipitator under vigorous stirring. The precipitation was obtained by centrifugation and washed with deionized water for three times. In the second step, under vigorous stirring the precipitation was slowly added into a florence flask full of the aqueous solution of NaF in the desired proportion. Subsequently, the mixture was heated slowly at 85°C in the oil bath for 24 hours. The $NaYbF_4$:0.8%Tm, 0.2%Nd sample of hexagonal phase was obtained through an alcohol ultrasonic dispersion process. Other samples with the molar compositions of $NaYb_{1-0.008-x}Tm_{0.008}Nd_xF_4$ ($x = 0.2\%$, 0.4%, 0.6%, 0.8%, and 1.2%) and $NaYb_{1-y}Tm_yF_4$ ($y = 0.2\%$, 0.4%, 0.6%, 0.8%, and 1.0%) can be synthesized in the same method. For comparison, the hexagonal β-$NaYF_4$:0.8%Tm sample was synthesized, also.

Structures of the samples were investigated by X-ray diffraction (XRD) using a D8 Advance equipment provided with Cu tube with K_α radiation at 1.54056 Å in the range of $10° \leq 2\theta \leq 70°$. Investigations on the particle size and morphology were performed with a transmission electron microscope (TEM) using a JEM-2100 scanning electron microscope (JEOL, Japan), equipped with an energy dispersive X-ray spectroscopy (EDS) system. The selected area electron diffractometer (SAED) attached on it operating at accelerating voltages up to 200 kV. Upconversion luminescence spectra excited by 808 nm laser were obtained in the R-500 Spectrophotometer made by Japan Spectroscopic CO, LTD. All the samples were pressed into circular pie with same size ($D = 5$ mm) and smooth surface. The beam was focused on the sample using a focal length lens of 2.5 cm and the fluorescence signal with the spot size of 1 mm. The signal of luminescence was detected at the angle of 90° with the incident beam. The dependence of upconverted emission intensity on pumping powers for different samples was obtained by changing the excitation powers. All above measurements were performed at room temperature.

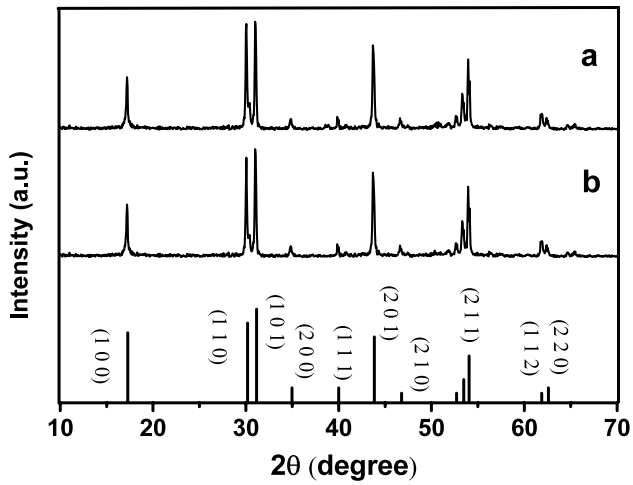

Fig. 1 XRD patterns of the (**a**) $NaYbF_4$:0.8%Tm and (**b**) $NaYbF_4$: 0.8%Tm, 0.6%Nd. *Bottom part* is the standard line pattern of the hexagonal phase β-$NaYbF_4$ (JCPDS 27-1427)

3 Results and discussions

3.1 Morphology and structure

Figure 1 illustrates the typical XRD patterns of $NaYbF_4$: 0.8%Tm and $NaYbF_4$:0.8%Tm, 0.6%Nd. The samples show a typical hexagonal phase β-$NaYbF_4$ structure, which accords basically with the standard X-ray diffraction JCPDS 27-1427. The fact that the NdF_3 and TmF_3 are not detected from X-ray diffraction patterns, suggests that the Nd^{3+} and Tm^{3+} well replaced Yb^{3+} sites in $NaYbF_4$ through the nonclosed hydrothermal synthetic method. The bulk hexagonal $NaYbF_4$ is in the space group of P6 (168) and its unit cell dimensions are $a = 5.929$ Å, $c = 3.471$ Å, and $v = 105.56$ Å^3, which is very similar to the structure of hexagonal phase β-$NaYF_4$ (JCPDS 16-0334) [17–19, 21–25]. The cell parameters $a = 5.945$ Å, $c = 3.478$ Å and $v = 106.428$ Å^3 of the $NaYbF_4$:0.8%Tm, 0.6%Nd sample can be calculated

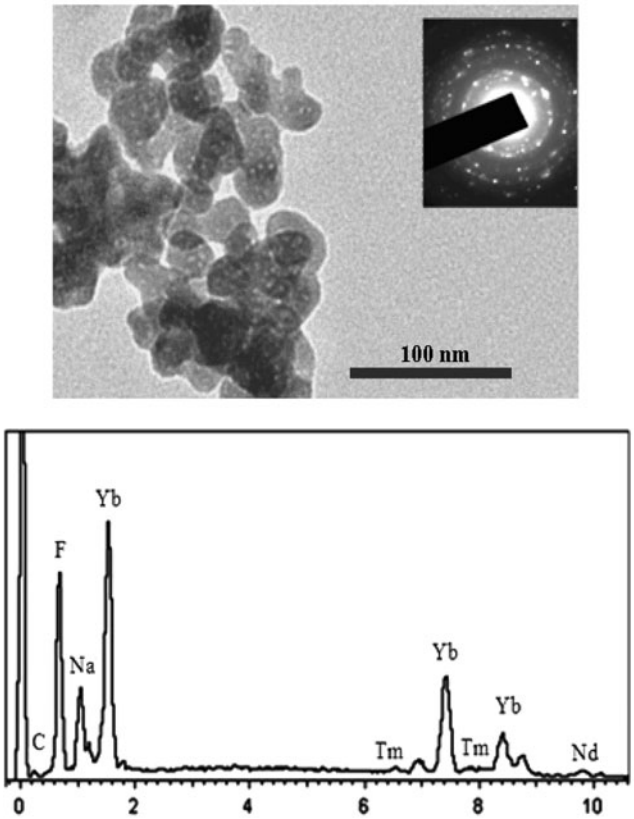

Fig. 2 TEM micrograph, SAED pattern, and EDS of the β-$NaYbF_4$: 0.8%Tm, 0.6%Nd sample

in terms of the X-ray diffraction data, which suggests that the lattice constant of hexagonal $NaYbF_4$ crystallites prepared in the experiment hardly varies compared with the bulk counterpart.

The TEM image of β-$NaYbF_4$:0.8%Tm, 0.6%Nd sample in Fig. 2 illustrates that sphere-like nanophosphors sized $35 \sim 45$ nm are distributed. Continuous diffraction rings are clearly seen in the SAED pattern that further indicates nanosized crystalline nature of the hexagonal phase $NaYbF_4$ sample. The crystallite size was estimated following the Debye–Scherrer equation [29]:

$$D = 0.89\lambda/\beta\cos\theta, \tag{1}$$

where D is the crystallite size, λ (nm) represents the wavelength of the X-ray, θ is the Bragg angle of the X-ray diffraction peak, and β represents the corrected half width of the diffraction peak. For the $NaYbF_4$:0.8%Tm, 0.6%Nd powder, the average crystals size $D = 40$ nm is calculated according to the Debye–Scherrer equation. The corresponding energy dispersive X-ray spectroscopy analysis (EDS) revealed that the main elemental components are Na, Yb, and F. In addition, the doped ion of Tm and Nd was also found in the EDS, which showed that the Tm and Nd element was doped into the $NaYbF_4$ powder.

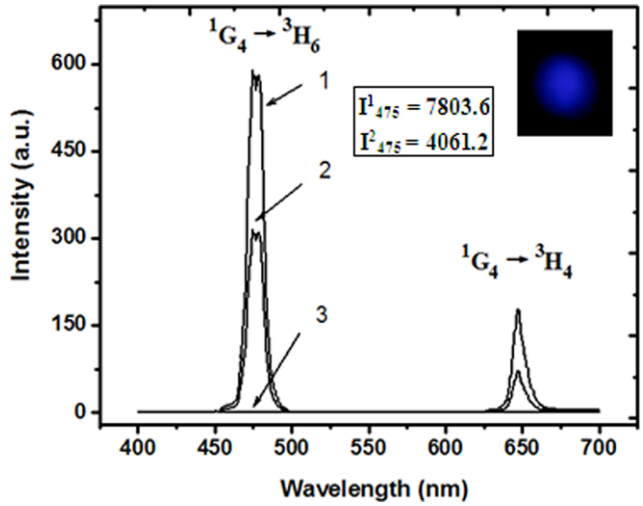

Fig. 3 Room-temperature frequency upconversion emission spectra of the (*1*) β-$NaYbF_4$:0.8%Tm, 0.6%Nd, (*2*) β-$NaYbF_4$:0.8%Tm, and (*3*) β-$NaYF_4$:0.8%Tm samples under 808 nm excitation. The *insert* is a photograph of the $NaYbF_4$:0.8%Tm, 0.6%Nd sample under 808 nm excitation with power of 250 mW

3.2 Photoluminescence

Figure 3 shows typical upconversion emission spectra at room temperature associated with Tm^{3+} as luminescence center under 808 nm excitation. For β-$NaYbF_4$:0.8%Tm, 0.6%Nd and β-$NaYbF_4$:0.8%Tm samples, the spectra exhibit the two distinct bands centered on 475 nm and 646 nm, corresponding to $^1G_4 \rightarrow {}^3H_6$ and $^1G_4 \rightarrow {}^3H_4$ transitions of Tm^{3+}, respectively. The ratio of integrated intensity of 475 nm and 646 nm is in the order of 4:1. It is observed that the presence of Nd^{3+} in the system, produces about two-fold enhancement in the blue and red emissions, as compared to the $NaYbF_4$:0.8%Tm sample. For the $NaYbF_4$:0.8%Tm, 0.6%Nd sample, the blue is strong enough to be clearly seen by the naked eyes with the pump power of 1 W/cm^2, as shown by the insert of Fig. 3. However, no emission band of Tm^{3+} is found in β-$NaYF_4$:0.8%Tm sample, which indicates the dominant upconversion mechanisms for the β-$NaYbF_4$:Tm^{3+} and β-$NaYbF_4$:Tm^{3+}/Nd^{3+} nanophosphors are $Tm^{3+} \rightarrow Yb^{3+} \rightarrow Tm^{3+}$ and $Nd^{3+} \rightarrow Yb^{3+} \rightarrow Tm^{3+}$ energy transfer processes, respectively.

The dependences of blue and red emissions intensity on Tm^{3+} and Nd^{3+} concentration are investigated in Fig. 4 for β-$NaYbF_4$:Tm^{3+} and β-$NaYbF_4$:Tm^{3+}/Nd^{3+} samples under 808 nm excitation with a pump power of 200 mW. For the β-$NaYbF_4$:Tm^{3+}, the maximum blue and red emissions intensity is observed at Tm^{3+} concentration of 0.8 mol%. For the β-$NaYbF_4$:Tm^{3+}/Nd^{3+}, when Tm^{3+} concentration is fixed at 0.8 mol%, the blue and red intensity first increase gradually then decrease with Nd^{3+} concentration, exhibiting a maximum value at around 0.6 mol%.

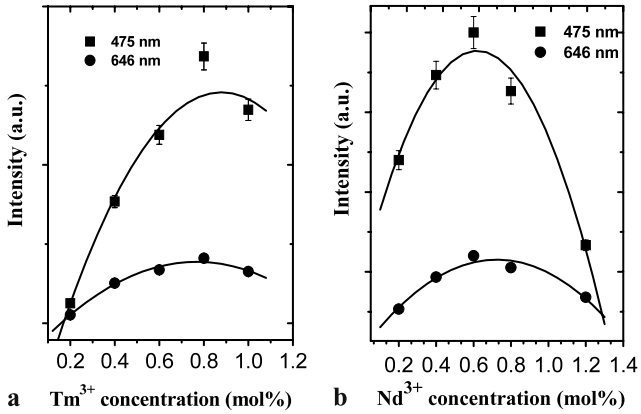

Fig. 4 Dependences of blue and red emissions intensity on (**a**) Tm^{3+} concentration for the $NaYb_{1-y}Tm_yF_4$ ($y = 0.2\%$, 0.4%, 0.6%, 0.8% and 1.0%) and (**b**) Nd^{3+} concentration for the $NaYb_{1-0.008-x}Tm_{0.008}Nd_xF_4$ ($x = 0.2\%$, 0.4%, 0.6%, 0.8%, and 1.2%) samples under 808 nm excitation

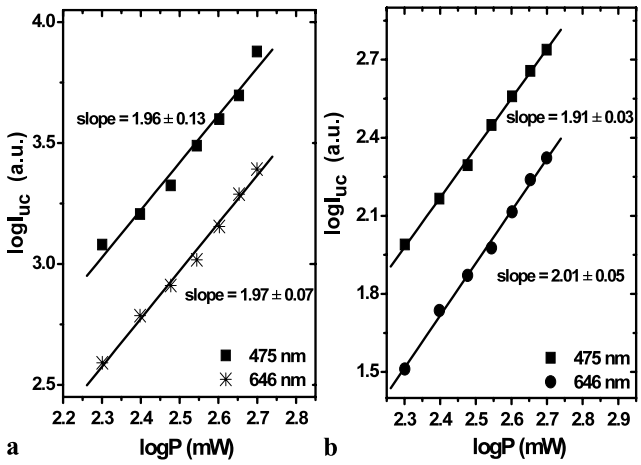

Fig. 5 Double-logarithmic plots of excitation power dependence of blue and red upconversion emissions intensity for the (**a**) β-$NaYbF_4$:0.8%Tm, 0.6%Nd and (**b**) β-$NaYbF_4$:0.8%Tm samples under 808 nm excitation

3.3 Upconversion mechanisms

The visible upconversion emission intensity I_{up} is proportional to the Nth power of the infrared pumping power P:

$$I_{up} \infty P^N, \tag{2}$$

where $N = 1, 2, 3, \ldots$ is the order of multiphoton transitions being the number of infrared quanta absorbed per one visible photon emission [30, 31]. The dependence of blue and red upconversion intensity upon excitation power was examined and about quadratic power law behavior was obtained, as portrayed in Fig. 5. In Fig. 5(a), the results indicate that two pump photons participate in the upconversion excitation mechanism and they excite Nd^{3+} and Tm^{3+} through the ground-state absorption (GSA) and energy transfer (ET).

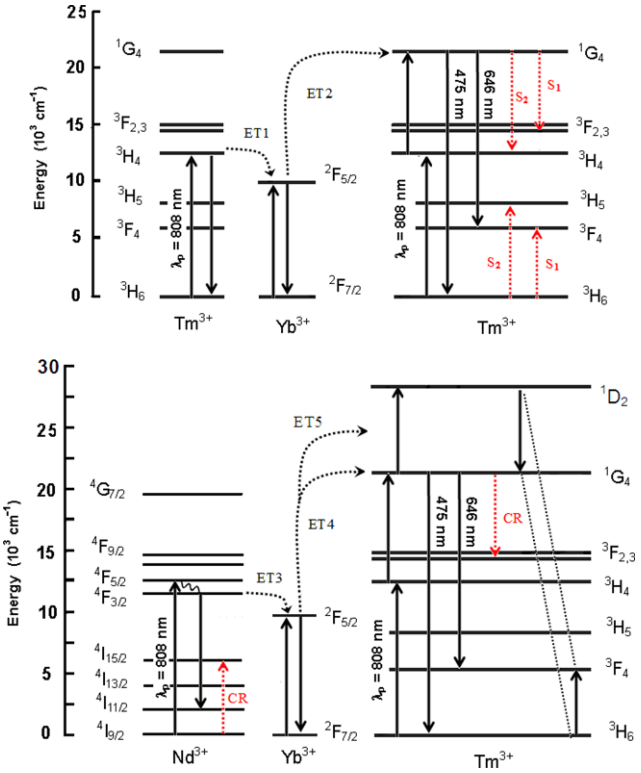

Fig. 6 Energy level diagrams of the Nd^{3+}, Tm^{3+} and Yb^{3+} ions and upconversion mechanisms for Tm^{3+}–Yb^{3+}–Tm^{3+} and Nd^{3+}–Yb^{3+}–Tm^{3+} systems under 808 nm excitation

Figure 5(b) illustrates that two pump photons participate in the upconversion excitation mechanism and they excite Tm^{3+} through GSA and ET.

In Cantelar and Dussardier's works [24, 32], the Tm^{3+} ion can emit blue emission alone in the $LiNbO_3$ and glass materials through the successive upconversion process of Tm^{3+} itself under 795 nm and 800 nm excitation. However, it is impossible in our work to generate blue emission by the GSA and excited-state absorption (ESA) of Tm^{3+} under 808 nm excitation, because no emission band of Tm^{3+} is observed in the spectrum of β-$NaYF_4$:0.8%Tm in Fig. 3. Thus, two possible upconversion mechanisms for β-$NaYbF_4$:Tm^{3+} and β-$NaYbF_4$:Tm^{3+}/Nd^{3+} are proposed in Fig 6. For β-$NaYbF_4$:Tm^{3+}, one Tm^{3+} ion in the ground state $^3H_6(Tm^{3+})$ is excited to excited state $^3H_4(Tm^{3+})$ after absorbs an 808 nm photon radiation. A nonresonant energy transfer between Tm^{3+} and Yb^{3+} occurs by the channel ET1

$$^3H_4(Tm^{3+}) + {}^2F_{7/2}(Yb^{3+}) \rightarrow {}^3H_6(Tm^{3+}) + {}^2F_{5/2}(Yb^{3+}), \tag{3}$$

which makes excited state $^2F_{5/2}(Yb^{3+})$ populated. At the same time, another Tm^{3+} ion absorbs an 808 nm photon, provoking the $^3H_6 \rightarrow {}^3H_4$ transition of Tm^{3+}. Subsequently, the energy on Yb^{3+} is transferred to $^3H_4(Tm^{3+})$,

resulting in the $^1G_4(Tm^{3+})$ excitation by the channel ET2

$$^2F_{5/2}(Yb^{3+}) + {}^3H_4(Tm^{3+}) \rightarrow {}^2F_{7/2}(Yb^{3+}) + {}^1G_4(Tm^{3+}). \quad (4)$$

And then the 4f electrons on $^1G_4$ state radiatively relax to the $^3H_6$ and $^3F_4$ states, giving blue (475 nm) and red (646 nm) upconversion luminescence.

For β-NaYbF$_4$:Tm^{3+}/Nd^{3+}, the 808 nm pump photons promote $^4I_{9/2}(Nd^{3+})$ to $^4F_{5/2}(Nd^{3+})$ by means of a GSA process. The Nd^{3+} at $^4F_{5/2}$ level relaxes nonradiactively to $^4F_{3/2}(Nd^{3+})$, and transfers resonantly its energy to a nearby Yb^{3+} at the $^2F_{7/2}$ ground state by the channel ET3

$$^4F_{3/2}(Nd^{3+}) + {}^2F_{7/2}(Yb^{3+}) \rightarrow {}^4I_{11/2}(Nd^{3+}) + {}^2F_{5/2}(Yb^{3+}). \quad (5)$$

The excited Yb^{3+} then transfer resonantly its energy to the $^3H_4(Tm^{3+})$ after excited by the second pump photon around 808 nm by the channels ET4

$$^3H_6(Tm^{3+}) + 808\ \text{nm}\ h\nu \rightarrow {}^3H_4(Tm^{3+}) \quad \text{(GSA)}, \quad (6)$$

$$^2F_{5/2}(Yb^{3+}) + {}^3H_4(Tm^{3+}) \rightarrow {}^2F_{7/2}(Yb^{3+}) + {}^1G_4(Tm^{3+}). \quad (7)$$

The Tm^{3+} radiatively relaxes from $^1G_4$ to the $^3H_6$ ground state, generating intense fluorescence signal around 475 nm. The red emission band around 646 nm is assigned to the $^1G_4 \rightarrow {}^3F_4$ transition.

In Zhang's work [33], the $^1D_2$ state of Tm^{3+} can be populated by the channel $^1G_4(Tm^{3+}) + {}^3F_4(Tm^{3+}) \rightarrow {}^1D_2(Tm^{3+}) + {}^3H_6(Tm^{3+})$, due to the saturation effect on the excitated $^1G_4$ state. The 450 nm blue emission can be switched through above energy transfer. However, the 450 nm blue emission is not observed in our samples. The channel $^1D_2(Tm^{3+}) + {}^3H_6(Tm^{3+}) \rightarrow {}^1G_4(Tm^{3+}) + {}^3F_4(Tm^{3+})$ occurs if the $^1D_2$ state is populated through ET5: $^2F_{5/2}(Yb^{3+}) + {}^1G_4(Tm^{3+}) \rightarrow {}^2F_{7/2}(Yb^{3+}) + {}^1D_2(Tm^{3+})$.

According to the Miyakawa–Dexter theory [34], the probability of phonon-assisted energy transfer (*ET*) is expressed as

$$W_{ET} = W_{ET}(0)\exp(-\beta\Delta E), \quad (8)$$

where ΔE is an energy gap between the energy levels of the donor and acceptor, $W_{ET}(0)$ is the transfer rate when $\Delta E = 0$, and β is a function of effective phonon energy and electron–phonon coupling strength. The equation implies that the smaller the energy gap is, the faster the energy transfer occurs; the larger energy mismatch is, the smaller

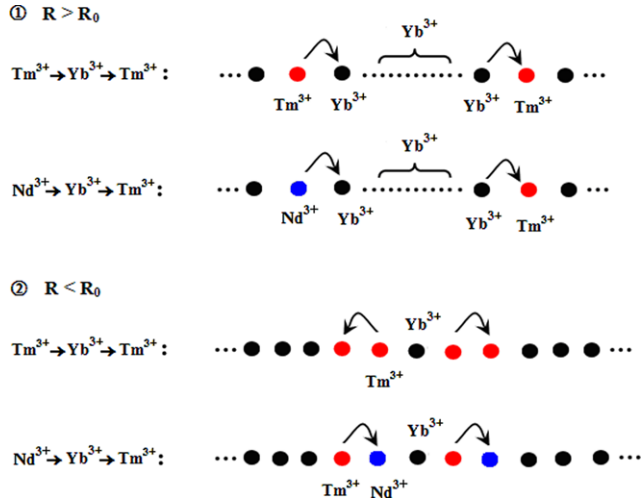

Fig. 7 A diagram of ideal energy transfer processes of excited ions in the Tm^{3+}–Yb^{3+}–Tm^{3+} and Nd^{3+}–Yb^{3+}–Tm^{3+} systems under 808 nm excitation

the energy transfer probability will be. For the *ET* process Tm^{3+} → Yb^{3+} → Tm^{3+}, the first step Tm^{3+} → Yb^{3+} in (3) exists at around energy mismatch of 2180 cm^{-1} and needs phonons to assist, whose probability will be smaller. However, the *ET* process Nd^{3+} → Yb^{3+} → Tm^{3+} is performed through two successive resonant energy transfers without assistant of phonons. Thus, the *ET* process Nd^{3+} → Yb^{3+} → Tm^{3+} is easier to carry out than the Tm^{3+} → Yb^{3+} → Tm^{3+} process. As a result, one can find that a onefold enhancement of blue and red emissions by introducing of Nd^{3+}.

3.4 Concentration quenching discussion

The energy transfer rate for dipole-dipole interaction can be expressed as

$$P_{SA}(R) = \frac{1}{\tau_s}\left(\frac{R_0}{R}\right)^6, \quad (9)$$

where τ_s is the actual lifetime of sensitizer excited, including multiphonon radioactive decay state. R_0 is the critical transfer distance for which excitation transfer and spontaneous deactivation of sensitizer have equal probabilities, and R is the distance between rear-earth ions [35, 36]. The dependence of blue and red emissions intensity on Tm^{3+} and Nd^{3+} concentration, as shown in Fig. 4, can be understood by the following consideration:

For the β-NaYbF$_4$:Tm^{3+}, when the Tm^{3+} doping concentration is much less than 0.8 mol%, the distance R between Tm^{3+} and Yb^{3+} is consistent with $R > R_0$, and the energy transfer process Tm^{3+} → Yb^{3+} → Tm^{3+} is blocked by Yb^{3+}–Yb^{3+} bridging ion pairs with high concentration, as portrayed in Fig. 7, resulting in small energy transfer

rate of $Tm^{3+} \rightarrow Yb^{3+} \rightarrow Tm^{3+}$ process. When the Tm^{3+} concentration is far more than 0.8 mol%, the distance R decreases and is consistent with $R < R_0$. The nonresonant energy transfer rate of $Tm^{3+} \rightarrow Yb^{3+}$ decreases and the resonant energy transfer $Tm^{3+} \rightarrow Tm^{3+}$ become active. It also can be explained in Fig. 6, the cross-relaxation (CR) processes of Tm^{3+}, S_1, and S_2, are the dominant methods to deplete excited level $^1G_4$, which are described in the following equations:

$$S_1: \quad {}^1G_4(Tm^{3+}) + {}^3H_6(Tm^{3+}) \rightarrow {}^3F_3(Tm^{3+}) + {}^3F_4(Tm^{3+}), \tag{10}$$

$$S_2: \quad {}^1G_4(Tm^{3+}) + {}^3H_6(Tm^{3+}) \rightarrow {}^3H_4(Tm^{3+}) + {}^3H_5(Tm^{3+}). \tag{11}$$

Obviously, the above energy transfers reduce the number of ions of $^1G_4$ excited state, as a result, the intensity of 475 nm and 646 nm emissions sharply decreases with high Tm^{3+} concentration.

For the β-$NaYbF_4$:Tm^{3+}/Nd^{3+}, when the Nd^{3+} concentration is much less than 0.6 mol%, the distance R between Nd^{3+} and Yb^{3+} is consistent with $R > R_0$, and the energy transfer process $Nd^{3+} \rightarrow Yb^{3+} \rightarrow Tm^{3+}$ is blocked by the Yb^{3+}–Yb^{3+} bridging ion pairs with high concentration, as portrayed in Fig. 7, resulting in a small energy transfer rate of $Nd^{3+} \rightarrow Yb^{3+} \rightarrow Tm^{3+}$ process. When the Nd^{3+} concentration is far more than 0.6 mol%, the distance R decrease and is consistent with $R < R_0$. The energy transfer rate of $Nd^{3+} \rightarrow Yb^{3+}$ decreases and the back energy transfer $Tm^{3+} \rightarrow Nd^{3+}$ become active. It also can be explained in Fig. 6; the resonant CR process of Tm^{3+} and Nd^{3+} plays role in depleting excited $^1G_4$ level, which is described in the following equation:

$$ {}^1G_4(Tm^{3+}) + {}^4I_{9/2}(Nd^{3+}) \rightarrow {}^3F_3(Tm^{3+}) + {}^4I_{15/2}(Nd^{3+}). \tag{12}$$

The above CR process depopulates the $^1G_4$ excited state, as a result, the intensity of 475 nm and 646 nm sharply decrease with high Nd^{3+} concentration.

4 Conclusion

The Tm^{3+} and Nd^{3+} doped β-$NaYbF_4$ nanophosphors were synthesized at 85°C in the air. The 85°C hydrothermal treatment replaces the high-temperature treatment process under HF atmosphere in solid-state reaction, and nonclosed synthesis avoids high pressure in traditional hydrothermal synthesis process. The blue and red upconversion emissions, originated from the $^1G_4 \rightarrow {}^3H_6$ and $^1G_4 \rightarrow {}^3H_4$ transitions of Tm^{3+}, were observed under 808 nm excitation. The blue emission intensity can be enhanced onefold by introducing Nd^{3+} in β-$NaYbF_4$:Tm^{3+}/Nd^{3+} nanophosphors. Intense blue emission has a potential application in three primary colors display and solid-state laser emitting in the blue spectral region. The dominant populating mechanisms for the β-$NaYbF_4$:Tm^{3+} and β-$NaYbF_4$:Tm^{3+}/Nd^{3+} nanophosphors are $Tm^{3+} \rightarrow Yb^{3+} \rightarrow Tm^{3+}$ and $Nd^{3+} \rightarrow Yb^{3+} \rightarrow Tm^{3+}$ energy transfer processes, respectively. The concentration quenching processes for blue and red emissions in β-$NaYbF_4$:Tm^{3+} and β-$NaYbF_4$:Tm^{3+}/Nd^{3+} nanophosphors are originated respectively from resonant CR processes of Tm^{3+} ions and resonant ET processes between Tm^{3+} and Nd^{3+} ions.

Acknowledgements This work was supported by National Natural Science Foundation of China (No. 51032002, No. 10874089, and No. 10704038) and Natural Science Foundation of Jiangsu Province (No. BK2008398) as well as the Project Innovation of Graduate Students of Jiangsu Province, China (Grant No. CX10B_095Z).

References

1. G.S. Yi, G.M. Chow, Adv. Funct. Mater. **16**, 2324 (2006)
2. S.Q. Man, E.Y.B. Pun, P.S. Chung, Appl. Phys. Lett. **77**, 483 (2000)
3. P.V. dos Santos, E.A. Gouveia, M.T. de Araujo, A.S. Gouveia-Neto, A.S.B. Sombra, J.A.M. Neto, Appl. Phys. Lett. **74**, 3607 (1999)
4. F. Lahoz, D.P. Shepherd, J.S. Wilkinson, M.A. Hassan, Opt. Commun. **281**, 3691 (2008)
5. G.S. Maciel, A. Biswas, R. Kapoor, P.N. Prasad, Appl. Phys. Lett. **76**, 1978 (2000)
6. V. Mahalingam, F. Mangiarini, F. Vetrone, V. Venkatramu, M. Bettinelli, A. Speghini, J.A. Capobianco, J. Phys. Chem. C **112**, 17745 (2008)
7. R. Balakrishnaiah, D.W. Kim, S.S. Yi, K. Jang, H.S. Lee, J.H. Jeong, Opt. Mater. **31**, 959 (2009)
8. F. Pandozzi, F. Vetrone, J.C. Boyer, R. Naccache, J.A. Capobianco, A. Speghini, M. Bettinelli, J. Phys. Chem. B **109**, 17400 (2005)
9. J.F. Suyver, A. Aebischer, D. Biner, P. Gerner, J. Grimm, S. Heer, K.W. Krämer, C. Reinhard, H.U. Güdel, Opt. Mater. **27**, 1111 (2005)
10. F. Güell, R. Solé, J. Gavaldà, M. Aguiló, M. Galán, F. Díaz, J. Massons, Opt. Mater. **30**, 222 (2007)
11. A.S. Gouveia-Neto, L.A. Bueno, R.F. do Nascimento, E.A. da Silva, Jr., E.B. da Costa, V.B. do Nascimento, Appl. Phys. Lett. **91**, 091114 (2007)
12. F. Lahoz, D.P. Shepherd, J.S. Wilkinson, M.A. Hassan, Opt. Commun. **281**, 3691 (2008)
13. E. Cantelar, G.A. Torchia, F. Cussó, J. Lumin. **122–123**, 459 (2007)
14. N.K. Giri, D.K. Rai, S.B. Rai, J. Appl. Phys. **104**, 113107 (2008)
15. A.S. Gouveia-Netoa, E.B. da Costa, P.V. dos Santos, L.A. Bueno, S.J.L. Ribeiro, J. Appl. Phys. **94**, 5678 (2003)
16. M. Schellhorn, S. Ngcobo, C. Bollig, Appl. Phys. B **94**, 195 (2009)
17. N. Coluccelli, G. Galzerano, L. Bonelli, A. Toncelli, A. Di Lieto, M. Tonelli P. Laporta, Appl. Phys. B **92**, 519 (2008)
18. X.F. Wang, S.G. Xiao, Y.Y. Bu, X.L. Yang, J.W. Ding, Opt. Lett. **33**, 2653 (2008)

19. J.C. Boyer, F. Vetrone, L.A. Cuccia, J.A. Capobianco, J. Am. Chem. Soc. **128**, 7444 (2006)
20. S. Heer, K. Kömpe, H. Güdel, M. Haase, Adv. Mater. **16**, 2102 (2004)
21. J.N. Shan, Y.G. Ju, Appl. Phys. Lett. **91**, 123103 (2007)
22. J.H. Zeng, J. Su, Z.H. Li, R.X. Yan, Y.D. Li, Adv. Mater. **17**, 2119 (2005)
23. L.Y. Wang, Y.D. Li, Chem. Mater. **19**, 727 (2007)
24. L.F. Liang, H. Wu, H.L. Hu, M.M. Wu, Q. Su, J. Alloy Compd. **368**, 94 (2004)
25. K.W. Krämer, D. Biner, G. Frei, H.U. Gudel, M.P. Hehlen, S.R. Luthi, Chem. Mater. **16**, 1244 (2004)
26. X.F. Wang, S.G. Xiao, Y.Y. Bu, X.L. Yang, J.W. Ding, J. Lumin. **129**, 325 (2009)
27. N. Menyuk, K. Dwight, J.W. Pierce, Appl. Phys. Lett. **21**, 159 (1972)
28. Z.Q. Li, Y. Zhang, Angew. Chem. Int. Ed. **45**, 7732 (2006)
29. A. Patra, C.S. Friend, R. Kapoor, P.N. Prasad, Chem. Mater. **15**, 3650 (2003)
30. A. Bednarkiewicz, W. Strek, J. Phys. D: Appl. Phys. **35**, 2503 (2002)
31. M. Pollnau, D.R. Gamelin, S.R. Luthi, H.U. Gudel, Phys. Rev. B **61**, 3337 (2000)
32. B. Dussardier, J. Wang, D.C. Hanna, D.N. Payne, Opt. Mater. **4**, 565 (1995)
33. Y.Y. Zhang, L.W. Yang, H.L. Han, J.X. Zhong, Opt. Commun. **282**, 2857 (2009)
34. J. Qiu, M. Shojiya, Y. Kawamoto, J. Appl. Phys. **86**, 909 (1999)
35. X. Wang, Y. Bu, S. Xiao, X. Yang, J.W. Ding, Appl. Phys. B **93**, 801 (2008)
36. F. Auzel, Chem. Rev. **104**, 139 (2004)